Acetonitrile Boosts Conductivity of Imidazolium Ionic Liquids

Vitaly V. Chaban,*,[†] Iuliia V. Voroshylova,[‡] Oleg N. Kalugin,[§] and Oleg V. Prezhdo[†]

[†]Department of Chemistry, University of Rochester, Rochester, New York 14627, United States
[‡]REQUIMTE, Departamento de Química e Bioquímica, Faculdade de Ciências, Universidade do Porto, 4169-007 Porto, Portugal
[§]Department of Chemistry, Kharkiv National University, Kharkiv 61077, Ukraine

Ⓢ *Supporting Information*

ABSTRACT: We apply a new methodology in the force field generation (*Phys. Chem. Chem. Phys.* **2011**, *13*, 7910) to study binary mixtures of five imidazolium-based room-temperature ionic liquids (RTILs) with acetonitrile (ACN). Each RTIL is composed of tetrafluoroborate (BF$_4$) anion and dialkylimidazolium (MMIM) cations. The first alkyl group of MIM is methyl, and the other group is ethyl (EMIM), butyl (BMIM), hexyl (HMIM), octyl (OMIM), and decyl (DMIM). Upon addition of ACN, the ionic conductivity of RTILs increases by more than 50 times. It significantly exceeds an impact of most known solvents. Unexpectedly, long-tailed imidazolium cations demonstrate the sharpest conductivity boost. This finding motivates us to revisit an application of RTIL/ ACN binary systems as advanced electrolyte solutions. The conductivity correlates with a composition of ion aggregates simplifying its predictability. Addition of ACN exponentially increases diffusion and decreases viscosity of the RTIL/ACN mixtures. Large amounts of ACN stabilize ion pairs, although they ruin greater ion aggregates.
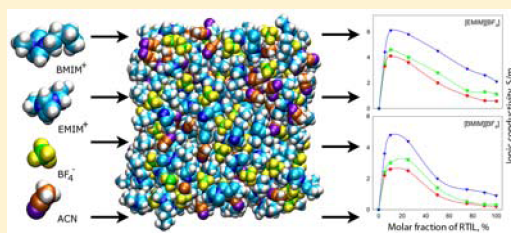
INTRODUCTION

Room-temperature ionic liquids (RTILs)[1−5] possess a set of remarkable properties for wide industrial applications. These unusual compounds are often referred to as alternative to traditional organic solvents. Due to negligible vapor pressure, unique permittivity, high thermal stability, nonflammability, solvation properties, and wide electrochemical window, RTILs are currently applied as reaction media, separation solvents, lubricants, and novel, efficient, and green electrolytes.[4−6]

Various RTILs were subjected to studies of fundamental physical, chemical, electrochemical, and photochemical properties during the past decade.[7−13] The electrical conductivity of certain pure RTILs and their solutions[5,7,14−20] has been studied over a wide temperature range. Most pure RTILs are extremely viscous (more than 50 cP at room temperature). As a result, they exhibit low self-diffusion (ca. 0.1×10^{-9} m^2 s^{-1}) and moderate conductivity (ca. 1 S m^{-1}). In order to enhance ion motion in RTILs, water and organic solvents can be admixed. The intermolecular and ion−molecular interactions, both mostly electrostatic in nature, drive dissociation of ion pairs, leading to greater ion mobility. A number of experimental and simulation studies of RTIL/water mixtures[20−23] have been conducted. In particular, recent work of Canongia Lopes et al.[24] presents a noteworthy cluster analysis, revealing the existence of four structural regimes—isolated water molecules, chain-like water aggregates, bicontinuous system, and isolated ions or small ion clusters. Importantly, the molar conductivity of these ion−molecular systems strongly depends on the admixture molar fraction. On the other hand, the amount of water in the RTIL/water mixtures can affect reaction rates, selectivity, media polarity, and solvation properties. Both cation and anion

diffusion grows in the RTIL/water mixtures thanks to the electrostatic interactions screening by molecular cosolvent.[20,25,26]

In contrast to RTIL/water mixtures, other potential cosolvents for RTILs are studied less extensively, although their importance is undoubted. In the present work, a novel methodology[27] is applied to investigate five RTIL/acetonitrile (ACN) mixtures. The cations are based on imidazole and contain ethyl (EMIM), butyl (BMIM), hexyl (HMIM), octyl (OMIM), and decyl (DMIM) groups. The anion (tetrafluoroborate, BF$_4$) is the same for all RTILs. Two more common RTILs, [EMIM][BF$_4$] and [BMIM][BF$_4$], with ACN (Figure 1) are investigated over the entire range of compositions at 283−323 K. Furthermore, three RTILs with longer alkyl tails, namely, hexyl, [HMIM][BF$_4$], octyl, [OMIM][BF$_4$], decyl, [DMIM][BF$_4$] (Table 1), which are usually missed in the electrochemistry-related research, are considered to study the role of cation size. ACN is a common aprotic solvent with a relatively high diffusion coefficient (4.3×10^{-9} m^2 s^{-1}) and low shear viscosity (0.34 cP). The structure and dynamics of pure ACN are driven by dipole−dipole interactions.[28] We predict this fact to be responsible for its outstanding miscibility with polar compounds, such as imidazolium-based RTILs.

We expect that mixing of [EMIM][BF$_4$], [BMIM][BF$_4$], [HMIM][BF$_4$], [OMIM][BF$_4$], and [DMIM][BF$_4$] with ACN leads to large changes in ion mobility, and therefore results in an increased conductivity. The molecular dynamics (MD)
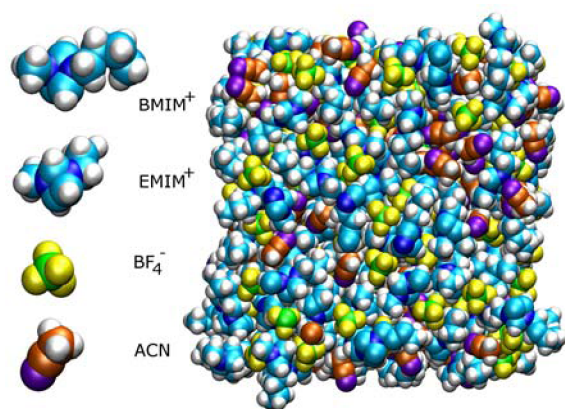
Figure 1. The simulated particles, 1-ethyl-3-methylimidazolium$^+$ (EMIM$^+$), 1-butyl-3-methylimidazolium$^+$ (BMIM$^+$), tetrafluoroborate$^-$ (BF$_4^-$), acetonitrile (ACN), and the simulated system of the equimolar mixture of [BMIM][BF$_4$] and ACN.

Table 1. The Number of Interacting Sites per System Consisting of the Five Imidazolium-Based RTILs and ACN[a]

x_1 (n_1/n_2)[b]	[EMIM][BF$_4$]	[BMIM][BF$_4$]	[HMIM][BF$_4$]	[OMIM][BF$_4$]	[DMIM][BF$_4$]
5 (15/285)	2070	2160	2250	2340	2430
10 (30/270)	2340	2520	2700	2880	3060
25 (75/225)	3150	3600	4050	4500	4950
50 (150/150)	4500	6300			
75 (225/75)	5850	7200			
90 (270/30)	6660	8280			
100 (300/0)	7200	9000	10800	12600	14400

[a]Each of these systems is equilibrated and simulated at 283, 298, and 323 K. [b]x_1 denotes a molar percentage of RTIL in a mixture, while n_1 and n_2 are the numbers of ion pairs and ACN molecules, respectively.

method with pairwise interaction potentials is applied to derive trajectories of 50 000 ps each. Our recent technique[27] exploiting uniformly scaled electrostatic charges is used to account for electronic polarization of RTILs. The available experimental densities and viscosities of the [EMIM][BF$_4$]/ACN[26,29] and [BMIM][BF$_4$]/ACN[20,26,30,31] are applied to validate our simulations. On the basis of the simulation results, we claim that the addition of the ACN allows for conductivity increase by 50 times. This occurs due to a unique balance of nonbonded interactions between the ions and ACN. For the first time, we show that conductivities only insignificantly depend on the cation size, shape, and mass. The demonstrated ability to enlarge the ionic conductivity of RTIL by varying the molar fraction of cosolvent favors oncoming applications of the RTIL/ACN mixtures.

■ METHODOLOGY

Simulation Setup. The phase trajectories for 26 systems (Table 1) are derived using classical MD simulations. Each system is considered at 283, 298, and 323 K. The simulations are accomplished using the modified version of the GROMACS 4.0 package[32−34] in the constant temperature constant pressure (NPT) ensemble. All molecular, ionic, and ion−molecular interactions are treated with pairwise interaction potentials. All atoms of RTILs and ACN (Figure 1) are represented as separate interaction centers, possessing Lennard-Jones (12,6) parameters and electrostatic charges. The constant temperature

is maintained using the velocity rescaling thermostat with a response time of 1.0 ps. The pressure coupling (1 bar) is done by the Parrinello−Rahman technique with a relaxation time of 4.0 ps. The leapfrog algorithm with a time-step of 1 fs is used to propagate equations of motion. The nearest neighbors list is updated every 10 time-steps within a sphere of 1.5 nm radius.

Slow internal dynamics of RTILs requires longer relaxation and production stages than in conventional MD studies (100−10 000 ps). This is also necessary for mixtures with small molar fractions of RTIL, since a lower amount of particles requires longer simulation times to achieve ergodicity. The initial relaxation is carried out at 350 K for 4000 ps in the constant volume constant temperature ensemble. Next, the generated systems are gradually cooled down to the target temperature (293, 298, and 323 K) for 2000 ps. The transport properties are derived from the 50 000 ps trajectories for each system. Three to five consequent MD trajectories of 50 000 ps are used to obtain reliable averages for ionic conductivity and shear viscosity. Each productive run begins with a random velocity distribution. In the latter case, the resulting trajectories are statistically independent and, therefore, can be treated using conventional statistical procedures.

The simulated systems (Table 1) are placed into cubic MD boxes (Figure 1) with periodic boundary conditions (PBC) to represent a bulk liquid. The electrostatic forces are treated by the particle mesh Ewald method[35] with a cutoff distance for the real-space component of 1.5 nm. The continuity of the Lennard-Jones potential is assured by using the shifted force method with a switch region between 1.2 and 1.3 nm.

Force Fields. A number of force fields (FFs) for RTILs have been suggested lately.[27,36−38] We recently demonstrated that realistic transport properties of RTILs can be obtained using a uniform decrease of the Coulombic interactions between all interaction sites.[27] Therefore, we borrow the parameters for imidazole ring atoms from ref 27 and the parameters for alkyl tails (which are not controversial) from the general-purpose AMBER FF.[39] Note, the neutral part of the alkyl tail does not require scaling to preserve compatibility with the available FFs for alkanes. The last published six-site model of Nikitin is used to simulate ACN. The model correctly reproduces density (773 kg m^{-3}), heat of vaporization (33.5 kJ mol^{-1}) structural distributions, and shear viscosity (~0.4 cP) of bulk ACN, as well as the corresponding properties of the ACN/water mixtures.[28] However, the diffusion constant at 298 K is underestimated (3.4 × 10^{-9} m^2 s^{-1}) compared to the experimental value (4.3 × 10^{-9} m^2 s^{-1}). This observation should be taken into account during the quantitative analysis of the transport properties of RTIL/ACN mixtures. Bonded and nonbonded interactions among all species are calculated via the equations proposed in the AMBER FF.[39]

Physical Properties. The properties are simulated by writing down atomic coordinates and interaction energies every 0.02 ps during 50 000 ps of each simulation. The ionic conductivity, shear viscosity, and cluster size distributions require an entire trajectory to achieve ergodicity. The diffusion constants are estimated using the last 3000 ps of each consequent MD run. All other properties can be derived using poorer sampling (1000 ps). The density of the RTIL/ACN mixtures (Figure 2) and its fluctuation during the simulation are estimated from the oscillations of the MD box volume in the NPT ensemble. Shear viscosity, η (Figure 3), is obtained by integrating the autocorrelation function of the off-diagonal elements of the pressure tensor. This method provides
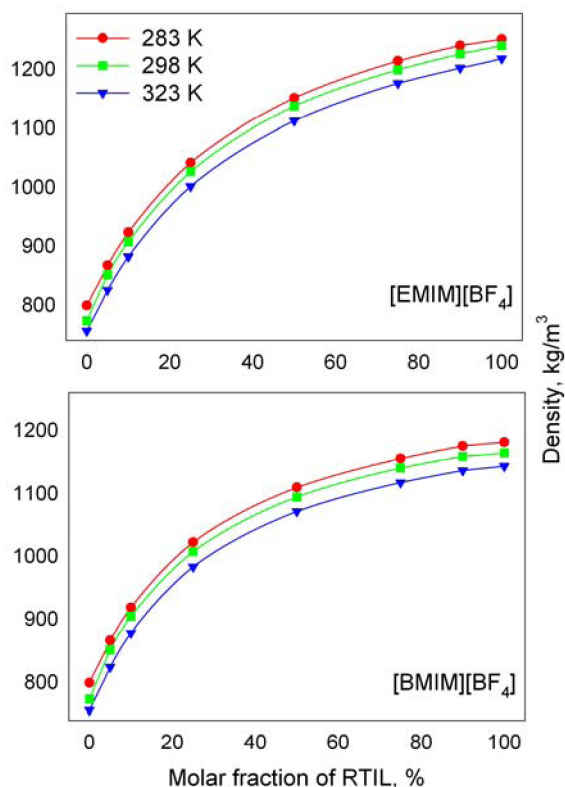
Figure 2. The specific density of $[EMIM][BF_4]$/ACN and $[BMIM]$-$[BF_4]$/ACN mixtures computed at 283 K (red circles), 298 K (green squares), and 323 K (blue triangles) as a function of molar fraction. The connecting lines are present to guide the eye.
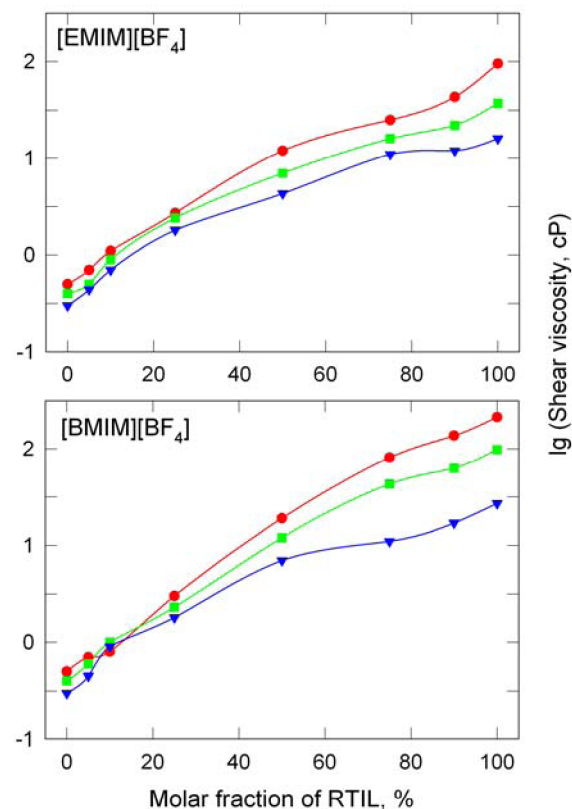

Figure 3. The shear viscosity of the $[EMIM][BF_4]$/ACN and $[BMIM][BF_4]$/ACN mixtures computed at 283 K (red circles), 298 K (green squares), and 323 K (blue triangles) as a function of molar fraction. The uncertainty does not exceed 20%. The connecting lines are present to guide the eye.

the viscosity of a system using equilibrium MD. However, extensive sampling is required due to huge pressure variations in a relatively small MD system. The diffusion constant (Figures 4 and 5), D, is computed by plotting mean square displacements of all atoms vs time. Ionic conductivity, σ (Figure 6), is obtained in the framework of the Einstein−Helfand formalism from the linear slope of mean-square displacements of the collective translational dipole moment. Importantly, this method requires PBC to be removed prior to computation; i.e., "free" diffusion should be considered. The corresponding formulas for transport properties are summarized elsewhere.[27] Radial distribution functions (Figure 9), $g_{ij}(r)$, are calculated following their classical definition from the MD trajectory parts of 1000 ps. Cluster analysis (Figures 10 and 11) is based on the single linkage approach. It postulates that two structures form a cluster, once they exhibit at least one direct contact, i.e., there is no other atom (including hydrogen)/ion/molecule between them. Next, another structure belongs to this same cluster, if it has at least one direct contact with any of these two structures. At each trajectory frame, the iterations persist, until no more structures can be added. In this study, we assume that two ions form a cluster, if the distance between the carbon (CR) site of $MMIM^+$ and the boron (B) site of BF_4^- does not exceed 0.500 and 0.512 nm (Figure 9) for $[EMIM][BF_4]$ and $[BMIM][BF_4]$. The above numerical criteria are exactly the positions of the first minima on the corresponding RDFs.

RESULTS AND DISCUSSION

The dependence of the specific density, ρ, of $[EMIM][BF_4]$ and $[BMIM][BF_4]$ upon x (RTIL) (Figure 2) is in good

Figure 4. The diffusion constants of cation ($EMIM^+$), anion (BF_4^-), and solvent molecules (ACN) and average diffusion constants of the $[EMIM][BF_4]$/ACN mixtures computed at 283 K (red circles), 298 K (green squares), and 323 K (blue triangles) as a function of molar fraction. The uncertainty does not exceed 10%. The connecting lines are present to guide the eye.
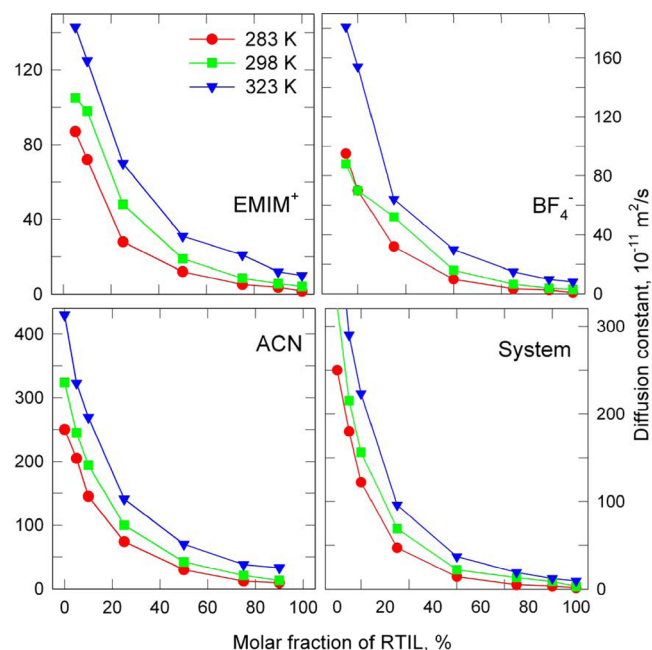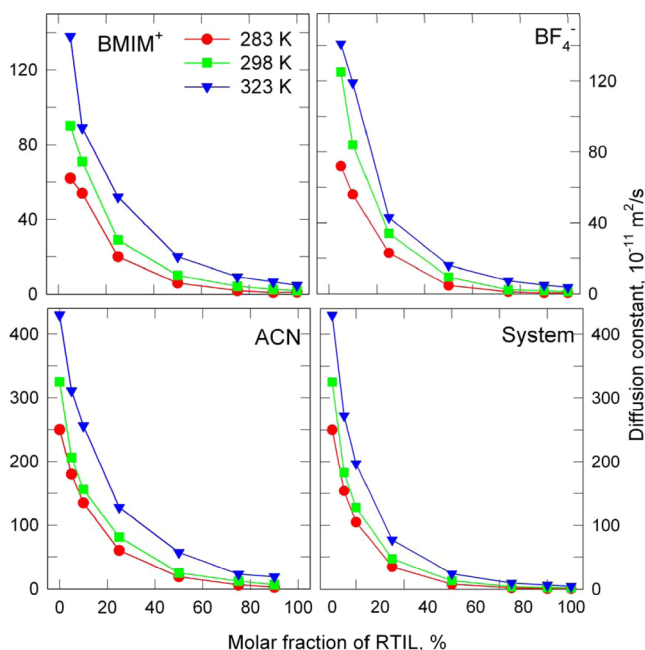
Figure 5. The diffusion constants of cation (BMIM$^+$), anion (BF$_4^-$), and solvent molecules (ACN) and average diffusion constants of the [BMIM][BF$_4$]/ACN mixtures computed at 283 K (red circles), 298 K (green squares), and 323 K (blue triangles) as a function of molar fraction. The uncertainty does not exceed 10%. The connecting lines are present to guide the eye.
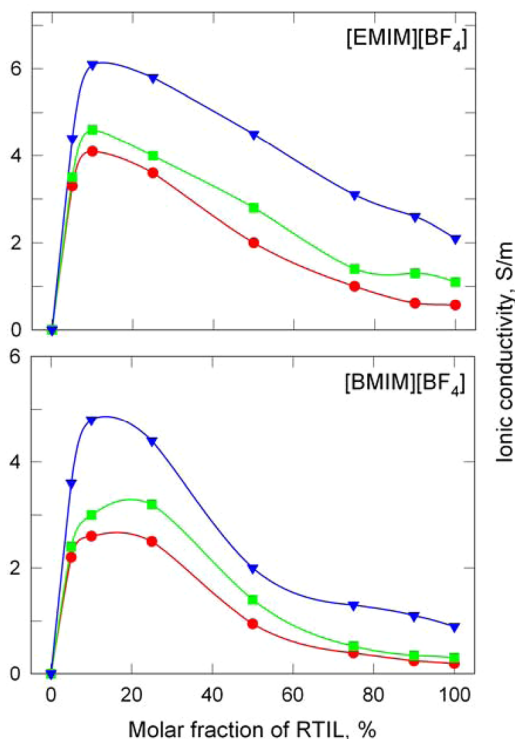

Figure 6. The ionic conductivity of the [EMIM][BF$_4$]/ACN and [BMIM][BF$_4$]/ACN mixtures computed at 283 K (red circles), 298 K (green squares), and 323 K (blue triangles) as a function of molar fraction. The uncertainty does not exceed 15%. The connecting lines are present to guide the eye.

agreement with the experimental values.[21,24−26] For instance, in the equimolar [BMIM][BF$_4$]/ACN mixture, the simulated

ρ_{298K} is 1094 kg m^{-3}. In turn, the experimental values range between 1102 and 1113 kg m^{-3}. Similarly, ρ ([EMIM][BF$_4$]/ACN)$_{50\%}$ = 1137 kg m^{-3} that is close to the experimental value of 1167 kg m^{-3}.[26] Provided that the fluctuations of ρ for this size of systems during MD simulation is ca. 10 kg m^{-3}, the accuracy of the simulated data is encouraging. A comprehensive comparison of our densities with the available experimental data for [BMIM][BF$_4$]/ACN mixtures at 298 and 232 K is provided in Figures S1 and S2 of the Supporting Information. The mixtures, containing [EMIM][BF$_4$], are slightly denser. First, the lyophobic alkyl tail interacts with the rest of the system less strongly compared to other moieties. Second, the fraction of heavy fluorine atoms in [EMIM][BF$_4$] is larger than that in [BMIM][BF$_4$]. Interestingly, at x (RTIL) < 25%, the difference between ρ ([EMIM][BF$_4$]) and ρ ([BMIM][BF$_4$]) vanishes. Provided that the size, mass, and shape of EMIM$^+$ and BMIM$^+$ are similar, we expect their diffusivities and conductivities to be close at these x (RTIL).

Shear viscosity, η (Figure 4), simultaneously reflects particle transport and energy dissipation in a system. The viscosities of [EMIM][BF$_4$]/ACN and [BMIM][BF$_4$]/ACN strongly depend on temperature. This trend is most pronounced when the molar fraction of RTIL exceeds 75%. For instance, at x ([BMIM][BF$_4$]) = 90%, η = 137 cP (283 K), 63 cP (298 K), and 17 cP (323 K). At the same compositions, η ([EMIM]-[BF$_4$]/ACN) is systematically higher than η ([EMIM][BF$_4$]/ACN). The observed distinction may contradict an intuition, since the density of [BMIM][BF$_4$]/ACN (Figure 2) is smaller. Furthermore, a longer lyophobic tail is expected to decrease negative nonideal deviations of properties. Hence, it should not cause an observed viscosity increase compared to [EMIM]-[BF$_4$]/ACN. On the other hand, BMIM$^+$ is 1.25 times heavier than EMIM$^+$, which results in a slower ion motion. It is additionally strengthened by an energetically very favorable solvation of cations by ACN. Approaching to its normal boiling point, ACN (η_{323K} = 0.2 cP) drastically decreases the viscosity of the entire system.

Our observations evidence that small admixtures of the aprotic solvents are not enough to approach RTIL-rich electrolytes to conventional electrolytes. Nevertheless, noticeable impact is achieved. The shear viscosity should be decreased down to 1−10 cP to enhance ionic conductivity for practical applications. This requirement is fulfilled as x (RTIL) is equal and less than 25% (Figure 3). One can admit that at these compositions ion dynamics is driven by ion−molecular interactions, in contrast to interionic ones. In most cases, the reported ηs are in good to excellent agreement with the experimental data provided elsewhere (Table S1 and Figure S3, Supporting Information).[20,26,30] Not only qualitative trends are reproduced, but also the numerical results are close. Note, the difference between experimental data reported by different authors is often larger than that between experiments and our simulations. This success encourages us to apply the same FF to derive other transport properties, particularly diffusion coefficients and ionic conductivities.

The shear viscosity of the system is in inverse proportion to its average diffusion coefficient, D, as suggested by the Einstein−Stokes relationship. This relationship holds rigorously, provided that the shape of the particles can be approximated by a sphere. Although this is not the case for imidazolium cations, we observe the qualitative trend. Figures 4 and 5 depict the average D's of the [EMIM][BF$_4$]/ACN and [BMIM][BF$_4$]/ACN mixtures, as well as the D's of all

components separately over the entire composition range at 283, 298, and 323 K. All D vs x(RTIL) dependences can be well described by exponential decay analytical functions with three parameters, $D = D_0 + A \exp(-B \times x(\text{RTIL}))$, where D_0 is the diffusion coefficient of the pure component and A and B are empirical constants. All correlation coefficients exceed 0.995, indicating a high accuracy of the derived data.

The ratio between the D's of the cation (EMIM$^+$, BMIM$^+$) and the anion changes drastically as x (RTIL) changes from 100 down to 0%. In pure RTILs and RTIL-rich mixtures, the diffusion of the anion, D_-, constitutes only 60–70% of the cation diffusion, D_+. This occurs in spite of the fact that cations are more branchy and weighty. The molecular masses of EMIM$^+$ and BMIM$^+$ are 111 and 139 amu, while the molecular mass of BF$_4^-$ is only 87 amu. At the same time, the bonds (B–F) of the anion are more polar bonds, resulting in strong interactions and hindered mobility. On the other hand, D (BF$_4^-$) grows faster with temperature than D (EMIM$^+$) and D (BMIM$^+$). For instance, the discussed D's are comparable at 400 K. The ratio is expected to invert at higher temperature. The same trend is observed as the molar fraction of ACN increases. At x (RTIL) $\geq$ 50%, the cation's D is larger; however, at x (RTIL) = 25%, the D_+/D_- ratio inverts. As x (RTIL) decreases down to 5%, D_- constitutes 110–130% of the D_+. Such a remarkable trend can be understood in terms of the ion–molecular peculiarities as follows. First, while the content of mobile ACN molecules is negligible, MMIM$^+$ and BF$_4^-$ create very large ion aggregates (Figures 10 and 11). Their structure is determined by strong Coulombic forces. The principal role belongs to the fluorine atoms of the anion and the hydrogen atoms of the imidazole ring (Figure 9). All anions are tightly bound to the neighboring cations, resulting in hindered transport (Figures 4–6) and excessive viscosity (Figure 3). As the molecular content increases, a certain amount of BF$_4^-$ is substituted by ACN molecules. The bulk D_{ACN} ((400–500) $\times 10^{-11}$ m^2 s^{-1}) is at least 2 orders of magnitude higher than D_{RTIL} ((1–5) $\times 10^{-11}$ m^2 s^{-1}). For instance, in the equimolar [BMIM][BF$_4$]/ACN mixtures, the average D's are 7.5, 13, and 24 ($\times 10^{-11}$ m^2 s^{-1}) at 283, 298, and 323 K. This is 1 order of magnitude higher than D's in pure [BMIM][BF$_4$]. Nearly the same ratio is observed for [BMIM][BF$_4$]/ACN mixtures, where the average D's are 14, 22, and 37 ($\times 10^{-11}$ m^2 s^{-1}) at 283, 298, and 323 K. At x (RTIL) < 25%, the large aggregates (Figures 10 and 11) are expected to vanish, resulting in an abrupt exponential growth of D's. Our findings are important for practical applications, since D's oversee those x (RTIL) at which ion motion is controlled by a cosolvent.

As we illustrated above, a drastic increase of the molecular and ion motion is expected as x(RTIL) is decreased down to 25% and less. The ionic conductivities, σ (Figure 6), of [EMIM][BF$_4$]/ACN and [BMIM][BF$_4$]/ACN confirm our finding. Indeed, 3–13 times increase of σ is observed upon dilution. The impact of ACN on σ ([BMIM][BF$_4$]/ACN) is noticeably larger than that on σ ([EMIM][BF$_4$]/ACN), 3–7 times vs 5–13 times. In order to understand this, we should accept that ion motion is driven by ACN at x (RTIL) $\geq$ 25%. For instance, at x (RTIL) < 10%, the average D's in [EMIM][BF$_4$]/ACN are 1.1–1.2 times larger than D's in [BMIM][BF$_4$]/ACN. Note, this ratio is equal to 2.5 in pure RTILs. We deduce that such σ is achieved due to a high mobility of cosolvent. The established trend is extremely important, since it allows for using arbitrary RTIL of the

imidazolium family for applications. The conductivity of pure RTILs greatly depends on the cation size (Tables S1 and S2, Supporting Information), being noticeably smaller for longer aliphatic tails. Our simulations predict the maximum of σ at the same narrow composition interval as recent experimental studies.[20,30] The results of Li et al.[30] are in somewhat better agreement with our data than the results of Zhu et al.[20] At x ([BMIM][BF$_4$]/ACN) = 50%, experimental σ is equal to 1.02 and 1.3 S m^{-1}, while the simulated σ is equal to 1.4 S m^{-1}. Systematical comparison between experimental and simulated conductivities over the entire composition range is provided in Figure S4 in the Supporting Information.

We report a strong correlation of conductivity with temperature. Whereas at 323 K σ ([EMIM][BF$_4$]/ACN) increases by 3 times upon dilution, its increase is 7 times at 283 K. For [BMIM][BF$_4$]/ACN, a similar trend is found, 5 and 13 times, respectively (Table S1, Supporting Information). Using mixtures is especially important for applications at T < 283 K. The correlation of σ with ion cluster composition is discussed below (Figures 10 and 11).

The observed trends are generalized by considering three more RTILs with longer alkyl tails, [HMIM][BF$_4$], [OMIM]-[BF$_4$], and [DMIM][BF$_4$]. The specific density and transport properties are depicted as a function of the tail size for 10 and 100% RTIL/ACN mixtures (Figure 7). The elongation of the lyophobic part of the cation leads to dynamics retardation, although the potential energy *per* atom decreases. This observation underlines that each $-$CH$_2-$ increment of the alkyl tail plays a significant role for imidazolium cations. In pure RTILs with octyl and decyl tails, D's and σ's are negligible (σ < 0.1 S m^{-1}), while the viscosities are extremely high (η > 400 cP at 283 K and η > 150 cP at 298 K). Liquid ACN boosts the ion transport drastically (Figure 7e), as its content approaches 10 mol %. For instance, σ ([DMIM][BF$_4$])$_{283K}$ = 0.029 S m^{-1}, while in the 10% mixture it is 1.8 S m^{-1}; i.e., 62 times increase is observed. The latter value is only 2.4 times smaller than σ ([EMIM][BF$_4$]) = 4.3 S m^{-1}. The trend is not so sharp (26 times increase) at 323 K but still very impressing. It largely depends on the fact that 283 K is below the glass transition temperature for the longest-tail RTILs. Thus, the solvation changes their phase to liquid. The ratio σ ([EMIM][BF$_4$]/ACN)/σ ([DMIM][BF$_4$]/ACN) is less than 2.4 times, whereas the ratio σ ([EMIM][BF$_4$])/σ ([DMIM][BF$_4$]) is 19–22 times at 283–323 K. The position of the conductivity maximum is invariable for all five RTILs. Note, x (RTIL) = 10% is a large concentration corresponding to 46 wt/wt % for the [DMIM]-[BF$_4$]/ACN mixture. This content has an amazingly tiny impact on the density, which differs by just 10–12 kg m^{-3}. In the case of pure RTILs, the corresponding density decrease is ca. 80 kg m^{-3} at 283–323 K.

Figure 8 summarizes the influence of ACN at 298–323 K. The increase of σ([EMIM][BF$_4$]/ACN) and σ ([BMIM]-[BF$_4$]/ACN) is much smaller than the increase of σ ([HMIM][BF$_4$]), σ ([OMIM][BF$_4$]), and σ ([DMIM][BF$_4$]). The corresponding difference at x (RTIL) = 25% is somewhat smaller, while for 5 and 10% it is nearly the same. Analyzing Figures 4–7 jointly, one can conclude that ion transport of all considered RTILs is driven by their affinity to ACN, rather than by the shape, mass, and polarity of RTILs. The binary mixtures of imidazolium-based RTILs and ACN form true solutions due to the exceptionally favorable interactions between components. The maximum σ ([BMIM][BF$_4$])$_{298K}$ = 1.9 S m^{-1} in butanone, 1.6 S m^{-1} in ethanol, 1.1 S m^{-1} in dichloromethane,
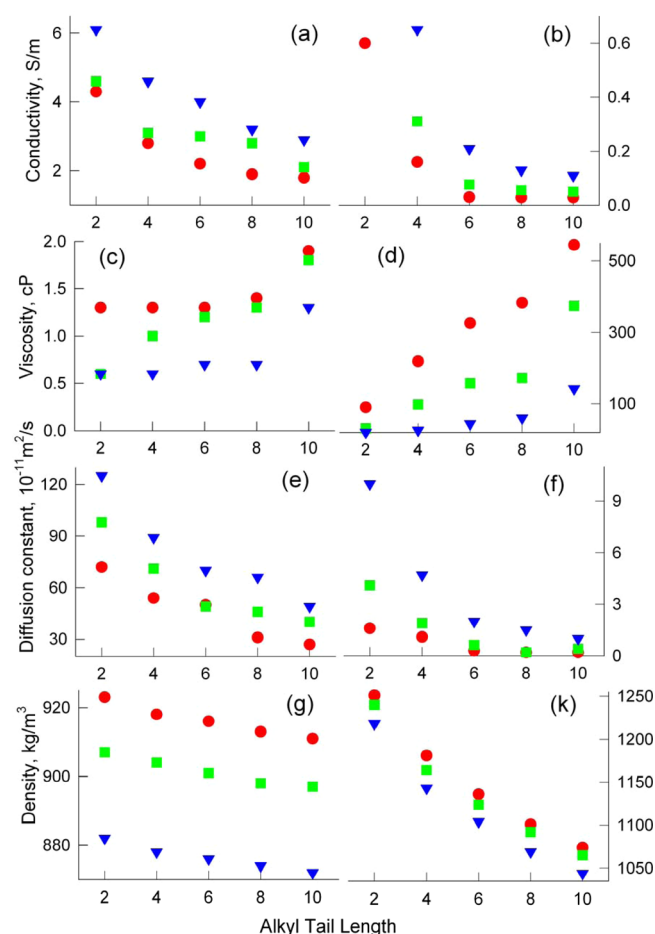
Figure 7. The ionic conductivity (a, b), shear viscosity (c, d), diffusion coefficient (e, f), and specific density (g, k) as a function of the number of carbon atoms forming the alkyl tail in 10% RTIL/ACN mixtures (a, c, e, g) and pure RTILs (b, d, f, k) at 283 K (red circles), 298 K (green squares), and 323 K (blue triangles). The connecting lines are present to guide the eye.
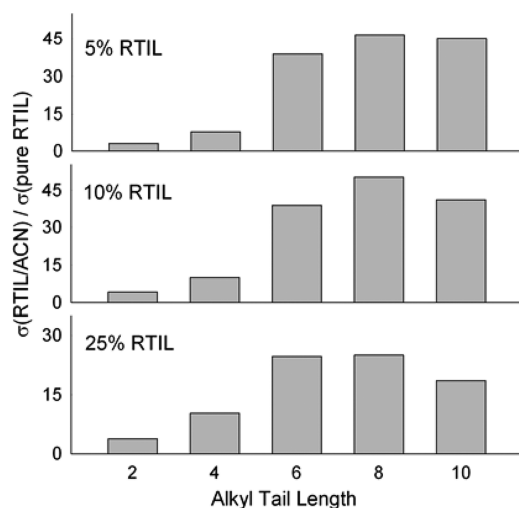

Figure 8. The ionic conductivity increase upon adding ACN at 298 K, expressed as a ratio of conductivity of 5, 10, and 25% RTIL/ACN mixtures, σ (RTIL/ACN), to conductivity of pure RTIL, σ (pure RTIL).

and 3.1 S m^{-1} in acetone (ACT). Additionally, it may be instructive to compare the simulated conductivities of [BMIM][BF$_4$]/ACN with those of [BMIM][TFSI], which are 0.68 S m^{-1} in 1-butanol, 2.6 S m^{-1} in methanol, 1.5 S m^{-1} in dichloroethane, and 4.4 S m^{-1} in ACN.[16] Clearly, ACN provides the largest increase of σ. Its effect can be compared only with ACT. In this context, investigation of longer-tailed RTIL/ACT mixtures can be of undoubted importance.

So far, [OMIM][BF$_4$]/ACN and [DMIM][BF$_4$]/ACN mixtures were not considered for electrochemistry, since their transport was believed to be unreasonably slow. However, in ACN-rich mixtures, ion motion is only moderately slower than that of the short-tailed RTILs. Our findings, therefore, open an exciting opportunity in tuning RTIL/ACN electrolyte solutions. Since common anions, such as BF$_4$, PF$_6$, or bis(trifluoromethanesulfonyl)-imide, demonstrate similar non-bonded interactions, it is natural to expect a like trend for these RTILs.

Radial distribution functions (Figure 9) between strongly interacting sites of cation and anion, $g_{CR-B}(r)$, are employed to
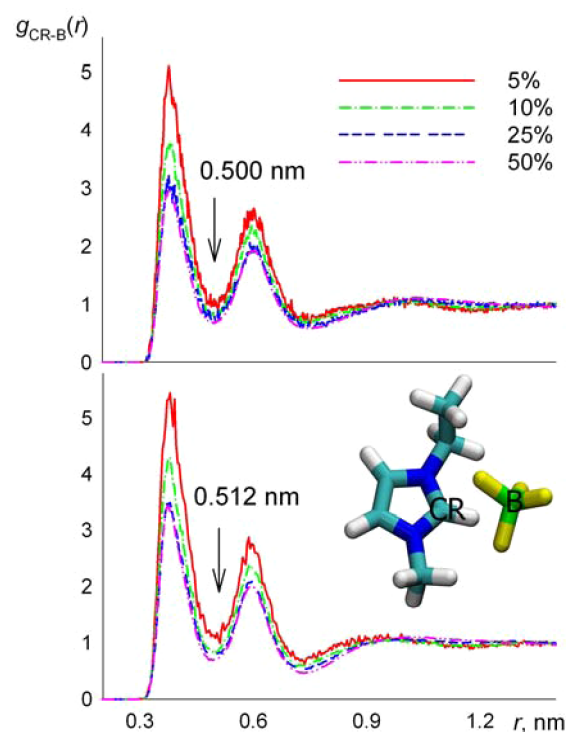

Figure 9. The radial distribution function, $g_{CR-B}(r)$, between the cation and the anion in the [EMIM][BF$_4$]/ACN (top) and [BMIM][BF$_4$]/ACN (bottom) mixtures as a function of molar fraction. The legend lists the molar fractions of RTIL in the mixtures.

derive distance criteria for cluster analysis (Figures 10 and 11). The position (0.38 nm), height (3–5), and shape of the first peak of $g_{CR-B}(r)$ predict the formation of the ion pairs at 5% < x (RTIL) < 50%. The probability of the ion pair formation is in direct proportion to the content of ACN. Consequently, ion–molecular interactions stabilize ion aggregates. The formation of neutral aggregates implies that conductivity decreases. A well pronounced second maximum at 0.59 nm with a height of 1.9–2.6 corresponds to larger aggregates. The cluster analysis suggests that the ion structures are very similar among imidazolium-based RTILs in ACN. First, the size of the biggest
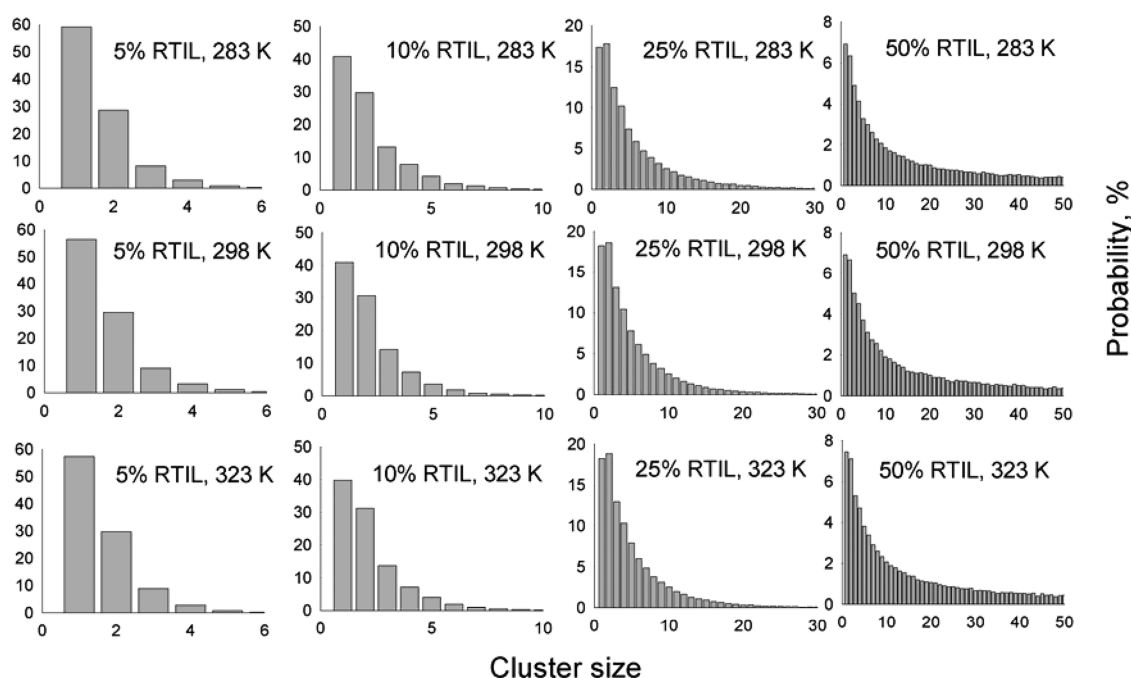
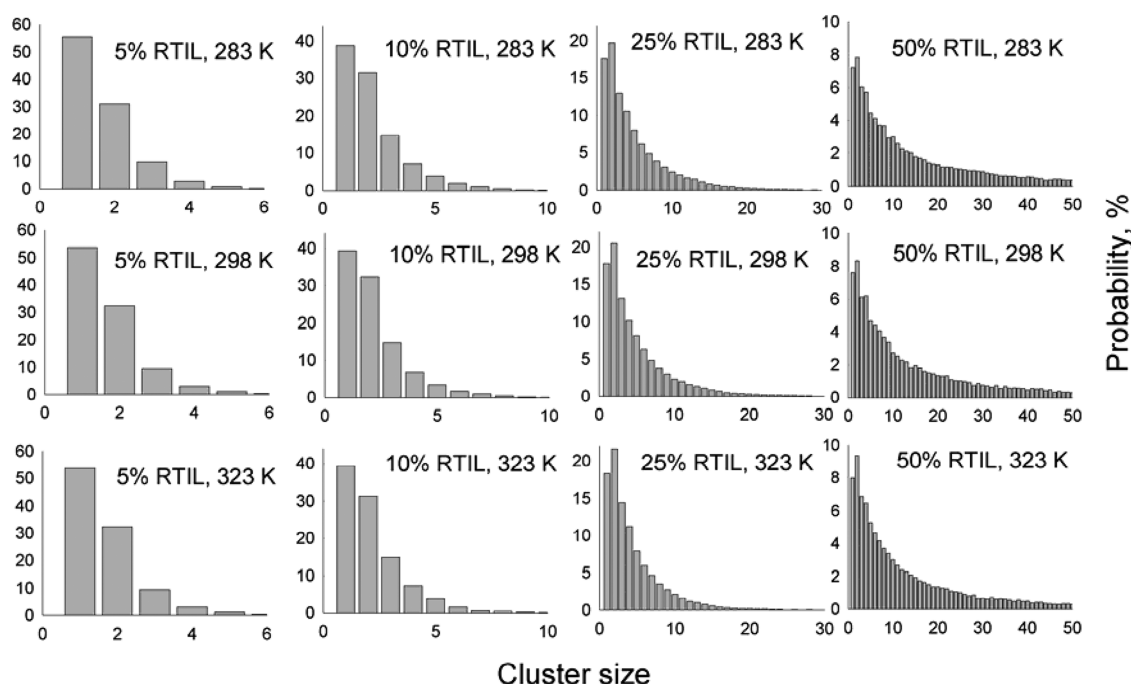**Figure 10.** The probability of ion aggregate formation in the $[EMIM][BF_4]/ACN$ mixtures at 283, 298, and 323 K.

Figure 11. The probability of ion aggregate formation in the $[BMIM][BF_4]/ACN$ mixtures at 283, 298, and 323 K.

aggregate is in direct proportion to x (RTIL). Second, the preferential aggregate is an ion pair, whose formation is more probable in ACN-rich mixtures. Third, significant percentages of free ions exist at x (RTIL) = 5–10% only. Interestingly, the amount of free ions is comparable with the amount of ion pairs at x (RTIL) = 25–50%. Thus, the ion pairs in these mixtures lack stability. As a result, a dynamical equilibrium between aggregates of varying composition is established.

The average size of the ion aggregate is 1.65, 2.16, 5.13, and 41.86 for 5, 10, 25, and 50% of $[EMIM][BF_4]$ at 298 K. The similar distribution is also observed for $[BMIM][BF_4]/ACN$, providing 1.67, 2.16, 4.86, and 19.13 for 5, 10, 25, and 50%,

respectively. The average sizes are summarized in Table 2. Whereas at x ($[RTIL][BF_4]$) = 5–10% the aggregate size is temperature independent, it strongly decreases as temperature increases in RTIL-richer mixtures, x ($[RTIL][BF_4]$) = 25–50%. We explain this by an enhanced mobility of ACN upon heating (Table S1, Supporting Information).

Another important observation is a systematic decrease of the average aggregate size in $[BMIM][BF_4]/ACN$ compared to $[EMIM][BF_4]/ACN$ at x (RTIL) > 10%. For instance, the difference between these two RTILs exceeds 2 times at x (RTIL) = 50%. Provided that $g_{CR-F}(r)$ for EMIM$^+$ and BMIM$^+$ (Figure 9) are very similar, such behavior may contradict an

Table 2. The Average Aggregate Sizes of $[EMIM^+]_n[BF_4^-]_m$ and $[BMIM^+]_n[BF_4^-]_m$ in Their Mixtures with ACN Derived from MD Simulations at 283, 298, and 323 K[a]

	$[EMIM][BF_4]$			$[BMIM][BF_4]$		
x (RTIL), %	283 K	298 K	323 K	283 K	298 K	323 K
5	1.59	1.65	1.61	1.63	1.67	1.71
10	2.23	2.16	2.22	2.22	2.16	2.17
25	5.69	5.13	5.14	4.95	4.86	4.42
50	45.30	41.86	34.56	21.24	19.13	16.49

[a]Note that the shown size is a sum of counterions, i.e., $n + m$.

intuition. By analyzing the probability of formation vs cluster size (Table 3), we found that $BMIM^+$ and BF_4^- tend to create a

Table 3. The Probabilities of the Formation of $[EMIM^+]_n[BF_4^-]_m$ and $[BMIM^+]_n[BF_4^-]_m$ Ion Aggregates in Their Equimolar Mixtures with ACN Derived from MD Simulations at 323 K

cluster size, (number of ions)	probability, %		cluster size, (number of ions)	probability, %	
	$[EMIM]$ $[BF_4]$	$[BMIM]$ $[BF_4]$		$[EMIM]$ $[BF_4]$	$[BMIM]$ $[BF_4]$
1−10	41.70	54.88	91−100	2.39	0.50
11−20	14.14	19.10	101−110	2.00	0.29
21−30	8.44	9.78	111−120	1.76	0.16
31−40	5.97	5.81	121−130	1.50	0.13
41−50	4.66	3.49	131−140	1.14	0.12
51−60	3.97	2.42	141−150	1.09	0.07
61−70	3.45	1.57	151−160	0.79	0.00
71−80	2.71	0.98	161−170	0.74	0.04
81−90	2.60	0.66	171−240	0.95	0.00

larger amount of smaller aggregates, while $EMIM^+$ and BF_4^- create larger aggregates. The largest aggregate consists of 240 and 170 ions for $[EMIM][BF_4]$ and $[BMIM][BF_4]$ at x (RTIL) = 50%. The probability of formation is negligible (ca. 0.01%). In turn, the largest clusters with a probability of more than 1% are 22 ions in $[EMIM][BF_4]$/ACN and 26 ions in $[BMIM]$-$[BF_4]$/ACN. The total amount of ions in this mixture (50% RTIL) is 300.

On the basis of the numerous *ab initio* calculations, it is recognized that imidazole rings of $EMIM^+$ and $BMIM^+$ possess similar properties.[3,40−42] Their tiny distinction (C_2H_4 group) leads to a noticeable difference in aggregate sizes but does not evince in local structure (RDFs). Since the alkyl tails do not exhibit any specific interactions with the environment, the smaller clusters in the cases of $BMIM^+$ and BF_4^- should be stipulated by steric factor exclusively. It is confirmed by the observation that the probability of the lonely ions is higher in $[BMIM][BF_4]$/ACN (7.98%) than in $[EMIM][BF_4]$/ACN (7.46%). Investigation of cluster formation in RTILs with longer alkyl tails may be helpful to understand the influence of chemically inert groups (CH_2) on the ionic subsystem.

An ability of charged particles to create large and long-lived ion aggregates is one of the principal factors which determine σ. The ionic species, belonging to a stable aggregate, move as a whole and possess smaller conductivity. Our results show that the average aggregate size is directly proportional to the content of ACN. As x (ACN) increases, the total number of charge carriers decreases. Thus, the position of conductivity maximum is determined by the interplay of the above two

factors. Interestingly, the position of the σ maximum coincides with x (RTIL), where the percentage of single ions exceeds the percentage of ion pairs. The ratio between the probabilities of these aggregates is inverse at larger x (RTIL). As the content of RTIL decreases down to 5%, the number of free ions increases; meanwhile, σ decreases. To summarize, σ is determined by the total concentration of charge carriers and not by the structure of the ionic subsystem at x (ACN) < 10%.

CONCLUSIONS

The dilution of RTILs with ACN is found to allow for conductivity increase by more than 50 times for long-tailed RTILs and more than 10 times for short-tailed RTILs. The ionic conductivity is a complex function of the mixture content, microscopic structure, and external conditions, whose assessment is not trivial without atomistic-precision description. Nevertheless, its maximum correlates well with a long-range ionic structure. The maximum is found at x (RTIL), where the number of free (not clusterized) ions exceeds the number of ion pairs. The dilution-driven conductivity increase is significantly larger for $[BMIM][BF_4]$ than for $[EMIM][BF_4]$, since the first one forms smaller ion clusters. The corresponding increase for $[DMIM][BF_4]$, $[OMIM][BF_4]$, and $[HMIM][BF_4]$ is even higher. Since the RTIL subsystem is driven by molecular cosolvent at x (RTIL) = 5−10%, the motion of all ions depends on the motion of ACN. The radial distribution functions show that molecular solvent stabilizes ion pairs, whereas the ion clusters of larger size are ruined, as suggested by our cluster analysis. The reliability of the reported data is justified by the available experimental densities, viscosities, and conductivities (see the Supporting Information).

ASSOCIATED CONTENT

Ⓢ Supporting Information
Tables S1 and S2 list the viscosities and conductivities of the imidazolium-based RTIL/ACN binary mixtures over a wide range of compositions. Figures S1−S4 provide a comparison between the simulated and available experimental data over the entire composition range. This material is available free of charge via the Internet at http://pubs.acs.org.

AUTHOR INFORMATION

Corresponding Author
*Phone: 1-585-276-5751. E-mail: v.chaban@rochester.edu, vvchaban@gmail.com.

Notes
The authors declare no competing financial interest.

ACKNOWLEDGMENTS

REFERENCES

(1) Rogers, R. D. *Nature* **2007**, *447*, 917−918.
(2) Earle, M. J.; Esperanca, J. M. S. S.; Gilea, M. A.; Lopes, J. N. C.; Rebelo, L. P. N.; Magee, J. W.; Seddon, K. R.; Widegren, J. A. *Nature* **2006**, *439*, 831−834.
(3) Hunt, P. A. *Mol. Simul.* **2006**, *32*, 1−10.
(4) Karadas, F.; Atilhan, M.; Aparicio, S. *Energy Fuels* **2010**, *24*, 5817−5828.

(5) Liu, H. T.; Liu, Y.; Li, J. H. *Phys. Chem. Chem. Phys.* **2010**, *12*, 1685−1697.

(6) Paulechka, Y. U. *J. Phys. Chem. Ref. Data* **2010**, 033108.

(7) Kashyap, H. K.; Annapureddy, H. V. R.; Raineri, F. O.; Margulis, C. J. *J. Phys. Chem. B* **2011**, *115*, 13212−13221.

(8) Shirota, H.; Castner, E. W. *J. Chem. Phys.* **2006**, *125*, 034904.

(9) English, N. J.; Mooney, D. A.; O'Brien, S. W. *J. Mol. Liq.* **2010**, *157*, 163−167.

(10) Hantal, G.; Partay, L. B.; Varga, I.; Jedlovszky, P.; Gilanyi, T. *J. Phys. Chem. B* **2007**, *111*, 1769−1774.

(11) English, N. J.; Mooney, D. A.; O'Brien, S. *Mol. Phys.* **2011**, *109*, 625−638.

(12) Castner, E. W.; Wishart, J. F.; Shirota, H. *Acc. Chem. Res.* **2007**, *40*, 1217−1227.

(13) Castner, E. W.; Margulis, C. J.; Maroncelli, M.; Wishart, J. F. *Annu. Rev. Phys. Chem.* **2011**, *62*, 85−105.

(14) Buchner, R.; Stoppa, A.; Hunger, J. *J. Chem. Eng. Data* **2009**, *54*, 472−479.

(15) Kowsari, M. H.; Alavi, S.; Najafi, B.; Gholizadeh, K.; Dehghanpisheh, E.; Ranjbard, F. *Phys. Chem. Chem. Phys.* **2011**, *13*, 8826−8837.

(16) Lopes, J. N. C.; Gomes, M. F. C.; Husson, P.; Padua, A. A. H.; Rebelo, L. P. N.; Sarraute, S.; Tariq, M. *J. Phys. Chem. B* **2011**, *115*, 6088−6099.

(17) Pinkert, A.; Ang, K. L.; Marsh, K. N.; Pang, S. S. *Phys. Chem. Chem. Phys.* **2011**, *13*, 5136−5143.

(18) Sanchez, E. M.; Ramirez, R. E.; Torres-Gonzalez, L. C.; Hernandez, A.; Garcia, A. *J. Phys. Chem. B* **2010**, *114*, 4271−4275.

(19) Takamuku, T.; Kyoshoin, Y.; Shimomura, T.; Kittaka, S.; Yamaguchi, T. *J. Phys. Chem. B* **2009**, *113*, 10817−10824.

(20) Zhu, A. L.; Wang, J. J.; Han, L. J.; Fan, M. H. *Chem. Eng. J.* **2009**, *147*, 27−35.

(21) Bester-Rogac, M.; Stoppa, A.; Hunger, J.; Hefter, G.; Buchner, R. *Phys. Chem. Chem. Phys.* **2011**, *13*, 17588−17598.

(22) Chen, T.; Chidambaram, M.; Lin, Z. P.; Smit, B.; Bell, A. T. *J. Phys. Chem. B* **2010**, *114*, 5790−5794.

(23) Modi, N.; Singh, P. R.; Mahendran, K. R.; Schulz, R.; Winterhalter, M.; Kleinekathofer, U. *J. Phys. Chem. Lett.* **2011**, *2*, 2331−2336.

(24) Bernardes, C. E. S.; Minas da Piedade, M. E.; Canongia Lopes, J. N. *J. Phys. Chem. B* **2011**, *115*, 2067−2074.

(25) Anouti, M.; Jacquemin, J.; Lemordant, D. *J. Chem. Eng. Data* **2010**, *55*, 5719−5728.

(26) Wang, J. J.; Tian, Y.; Zhao, Y.; Zhuo, K. *Green Chem.* **2003**, *5*, 618−622.

(27) Chaban, V. V.; Voroshylova, I. V.; Kalugin, O. N. *Phys. Chem. Chem. Phys.* **2011**, *13*, 7910−7920.

(28) Nikitin, A. M.; Lyubartsev, A. P. *J. Comput. Chem.* **2007**, *28*, 2020−2026.

(29) Stoppa, A.; Hunger, J.; Buchner, R. *J. Chem. Eng. Data* **2009**, *54*, 472−479.

(30) Li, W. J.; Zhang, Z. F.; Han, B. X.; Hu, S. Q.; Xie, Y.; Yang, G. Y. *J. Phys. Chem. B* **2007**, *111*, 6452−6456.

(31) Huo, Y.; Xia, S. Q.; Ma, P. S. *J. Chem. Eng. Data* **2007**, *52*, 2077−2082.

(32) Hess, B.; Kutzner, C.; van der Spoel, D.; Lindahl, E. *J. Chem. Theory Comput.* **2008**, *4*, 435−447.

(33) Van der Spoel, D.; Hess, B. *Wiley Interdiscip. Rev.: Comput. Mol. Sci.* **2011**, *1*, 710−715.

(34) Van der Spoel, D.; Lindahl, E.; Hess, B.; Groenhof, G.; Mark, A. E.; Berendsen, H. J. C. *J. Comput. Chem.* **2005**, *26*, 1701−1718.

(35) Essmann, U.; Perera, L.; Berkowitz, M. L.; Darden, T.; Lee, H.; Pedersen, L. G. *J. Chem. Phys.* **1995**, *103*, 8577−8593.

(36) Borodin, O. *J. Phys. Chem. B* **2009**, *113*, 11463−11478.

(37) Shimizu, K.; Almantariotis, D.; Gomes, M. F. C.; Padua, A. A. H.; Lopes, J. N. C. *J. Phys. Chem. B* **2010**, *114*, 3592−3600.

(38) Wu, X. P.; Liu, Z. P.; Huang, S. P.; Wang, W. C. *Phys. Chem. Chem. Phys.* **2005**, *7*, 2771−2779.

(39) Wang, J. M.; Wolf, R. M.; Caldwell, J. W.; Kollman, P. A.; Case, D. A. *J. Comput. Chem.* **2004**, *25*, 1157−1174.

(40) Danten, Y.; Cabaco, M. I.; Besnard, M. *J. Phys. Chem. A* **2009**, *113*, 2873−2889.

(41) Bhargava, B. L.; Saharay, M.; Balasubramanian, S. *Bull. Mater. Sci.* **2008**, *31*, 327−334.

(42) Tsuzuki, S.; Katoh, R.; Mikami, M. *Mol. Phys.* **2008**, *106*, 1621−1629.